ACSNANO
www.acsnano.org
ARTICLE

Resistive Switching Mechanisms on TaO_x and $SrRuO_3$ Thin-Film Surfaces Probed by Scanning Tunneling Microscopy

Marco Moors,[†,⊥] Kiran Kumar Adepalli,[‡,§,⊥] Qiyang Lu,[§] Anja Wedig,[†] Christoph Bäumer,[†] Katharina Skaja,[†] Benedikt Arndt,[†] Harry Louis Tuller,[§] Regina Dittmann,[†] Rainer Waser,[†,∥] Bilge Yildiz,*[,‡,§] and Ilia Valov*[,†,∥]

[†]Peter Grünberg Institut, Forschungszentrum Jülich, Wilhelm-Johnen-Straße, 52425 Jülich, Germany

[‡]Department of Nuclear Science and Engineering and [§]Department of Materials Science and Engineering, Massachusetts Institute of Technology, 77 Massachusetts Avenue, Cambridge, Massachusetts 02139, United States

[∥]Institut für Werkstoffe der Elektrotechnik 2, RWTH Aachen University, Sommerfeldstraße 24, 52074 Aachen, Germany

Supporting Information

ABSTRACT: The local electronic properties of tantalum oxide (TaO_x, $2 \leq x \leq 2.5$) and strontium ruthenate ($SrRuO_3$) thin-film surfaces were studied under the influence of electric fields induced by a scanning tunneling microscope (STM) tip. The switching between different redox states in both oxides is achieved without the need for physical electrical contact by controlling the magnitude and polarity of the applied voltage between the STM tip and the sample surface. We demonstrate for TaO_x films that two switching mechanisms operate. Reduced tantalum oxide shows resistive switching due to the formation of metallic Ta, but partial oxidation of the samples changes the switching mechanism to one mediated mainly by oxygen vacancies. For $SrRuO_3$, we found that the switching mechanism depends on the polarity of the applied voltage and involves formation, annihilation, and migration of oxygen vacancies. Although TaO_x and $SrRuO_3$ differ significantly in their electronic and structural properties, the resistive switching mechanisms could be elaborated based on STM measurements, proving the general capability of this method for studying resistive switching phenomena in different classes of transition metal oxides.

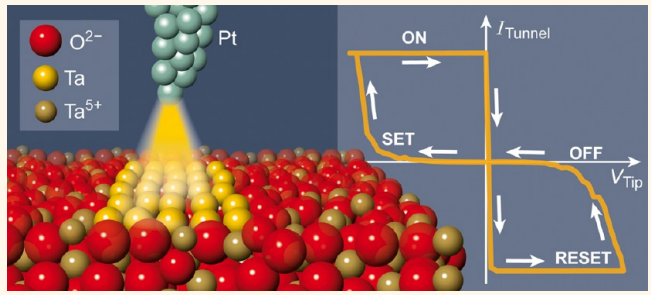

KEYWORDS: *resistive switching, strontium ruthenate, tantalum oxide, scanning tunneling microscopy, electric field effect*

Redox-based resistance switching random access memories (ReRAMs) are considered as the next-generation memory devices to replace the present flash-based technology.[1,2] ReRAMs have a simple metal–solid electrolyte–metal architecture, storing binary code information using the change in the resistance induced by filament formation and rupture, defining the low-resistive ON state (also denoted as LRS) and the high-resistive OFF state (or HRS), respectively.[3] High scalability, CMOS compatibility, switching times in the subnanosecond range, excellent endurance and retention, and low power consumption are key but otherwise difficult-to-duplicate features of ReRAM devices.[1−4] On the basis of the principle operation mechanisms of resistive switching, ReRAM devices are classified[3] into valence change memory (VCM), electrochemical metallization memory (ECM), and thermochemical memory (TCM) devices. Resistive switching in these devices is well understood to rely on redox reactions and migration of ionic species, causing either nanoconfined electronically conducting filaments percolating between the electrodes or, alternatively, laterally homogeneous active interfaces.[3,5]

In the past few years, a variety of oxide systems, *e.g.*, $SrTiO_3$, NiO, HfO_2, Ta_2O_5, or TiO_2, were shown to be promising for resistive switching,[3] but a detailed underlying microscopic picture, supported by a quantitative atomistic model, remains lacking. This is largely due to physical and technical challenges in analyzing the processes that take place locally at the atomic scale during switching.[6] However, significant progress is being made in that respect by use of high-resolution techniques such as *in situ* transmission electron microscopy (TEM),[7,8] 3D tomography,[9] local conducting atomic force microscopy (LC-AFM),[10−16] and scanning tunneling microscopy (STM).[17−19] STM provides the ultimate lateral resolution and a noncontact

Received: November 6, 2015
Accepted: January 7, 2016
Published: January 7, 2016

DOI: 10.1021/acsnano.5b07020
ACS Nano 2016, 10, 1481−1492

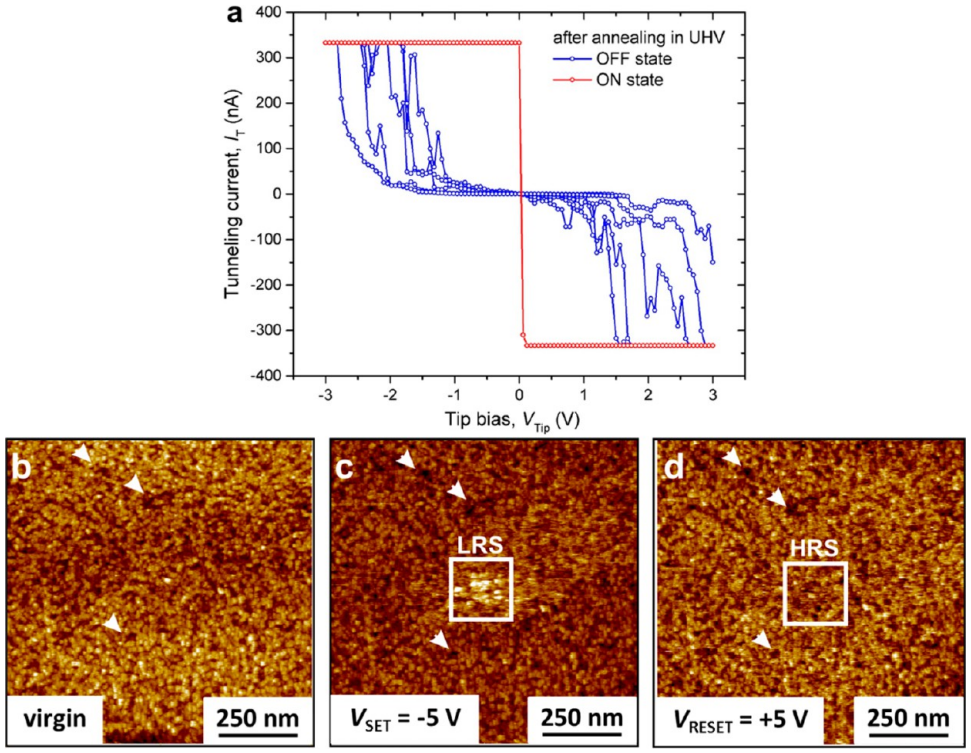

Figure 1. (a) *I*−*V* curves on bright regions corresponding to LRS (ON state) and on unmodified regions corresponding to HRS (OFF state) on TaO_x thin films after annealing in UHV. (b−d) STM images (1000 nm × 1000 nm, taken with V_{Tip} = −3.0 V and I_T = 0.5 nA) of the UHV-annealed TaO_x film (b) before and (c) after scanning the marked area at the center with V_{Tip} = −5.0 V; (d) after additionally scanning the marked area in (c) with V_{Tip} = +5.0 V. The arrows in (b), (c), and (d) show the features on the surface that are the same and, thus, used as fiducial markers in the consecutive images.

option for electrical manipulation of resistive switching materials. It facilitates high-resolution imaging of topographic features and enables detection of the early stages of the resistive switching process.[19] Furthermore, STM in the spectroscopy mode (STS) uncovers the electronic structure of devices, characterized by tunneling current−voltage (*I*−*V*) measurements. Use of STM for switching (*i.e.*, atomic switch) or device characterization has been largely restricted to samples with a sufficiently high electronic conductivity, *e.g.*, Ag_2S,[18] Cu_2S,[20] Nb-doped $SrTiO_3$,[21] or highly conducting regions on SiO_2.[22] However, recent studies have shown that STM can also be applied to atomic switch experiments on ion conductors[19] or even on materials considered as macroscopic insulators.[23] This can be done by increasing the electronic conductivity of the ionic conducting films, either by extrinsic doping or by thermal reduction, enabling quantum mechanical tunneling without significantly influencing the ionic processes. In this approach, we directly use the switching time as a kinetic parameter that is independent of the electronic properties[19] (in contrast to the current measured in two-electrode configurations).

In this work, we show combined STM/STS studies on the switching mechanisms in VCM-type ReRAM materials performed in a nondestructive and facile way. We chose the wide band gap TaO_x and the electronically conducting $SrRuO_3$ thin films as models for two distinctly different classes of oxides. TaO_x is a common switching layer in ReRAMs, and $SrRuO_3$ is a common electrode material. These oxides differ strongly in their physical and electrical properties; TaO_x can be considered as a mixed ionic−electronic conductor at the nanoscale (but macroscopic insulator), and $SrRuO_3$ is a highly electronically conducting material. We successfully showed area-wise (nm-scale) switching on both of these oxides (obtaining LRS and HRS) under applied electric fields and analyzed the corresponding electronic structures. We demonstrate that sample history and the polarity of the applied voltage play key roles in defining the dominant resistive switching mechanism. Investigating these materials that differ in resistive switching mechanisms represents the wide-ranging applicability of STM in the field of resistive switching. Our approach and results highlight the utility of *in situ* STM for studying the mechanism of resistive switching for all classes of ReRAM materials.

RESULTS AND DISCUSSION

Resistive Switching on TaO_x Induced by STM Tip. The TaO_x films were locally switched and examined by STM following two different treatment conditions: (i) annealing in ultrahigh vacuum (UHV) at 500 °C for approximately 2 h and (ii) exposure to ambient air following the procedure in (i). These two pretreatment conditions lead to different types of switching behavior at the surface of the films, as explained below.

As-deposited TaO_x ($x \approx 2.5$) films were highly insulating for STM imaging (see Figure S1a,b in supplementary data). Therefore, the films were reduced (formed) under a UHV atmosphere in the analysis chamber prior to imaging by STM, without exposure to ambient air. After the formation they could be switched to LRS/HRS by applying a voltage to the STM tip (Figure S1c).

It is important to note here that, in contrast to classical *I*−*V* measurements performed either with the aid of macroscopic needles or by an AFM cantilever in contact mode, the *I*−*V* data

DOI: 10.1021/acsnano.5b07020
ACS Nano 2016, 10, 1481−1492

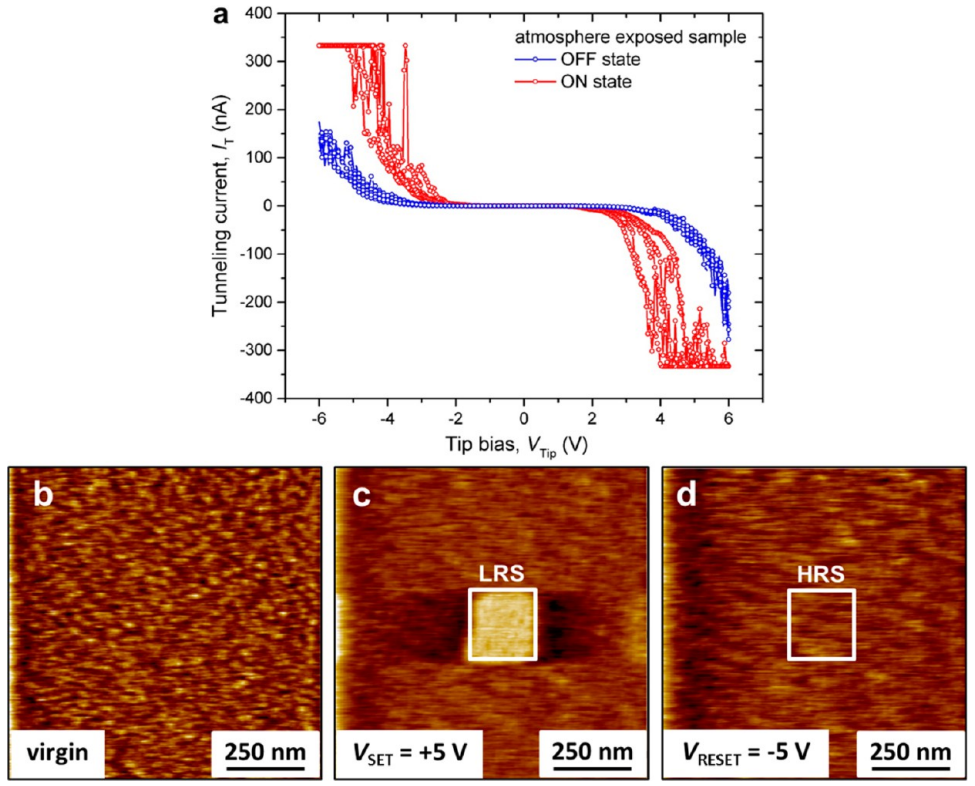

Figure 2. (a) $I-V$ curves on the bright regions corresponding to LRS and on the unmodified regions corresponding to the HRS on TaO_x thin films after annealing in UHV and exposing to the atmosphere. (b–d) STM images (1000 nm × 1000 nm, taken with V_{Tip} = −3.0 V and I_T = 0.5 nA) of the TaO_x sample after exposure to the atmosphere taken (b) before and (c) after scanning the marked area with V_{Tip} = +5.0 V; (d) after additionally scanning the marked area in (c) with V_{Tip} = −5.0 V.

from scanning tunneling spectroscopy do not represent the whole bulk resistance. This is due to the nature of STM measurements, where the current flow originates only from tunneling processes between the tip and the surface. Given the tunneling depth of electrons, only the first one or two atomic layers contribute meaningful information to the spectra. To a first approximation, the current reflects the degree of occupation of atomic orbitals with a component perpendicular to the surface, *e.g.*, the d_{z^2} orbital of transition metal atoms or the p_z orbital of oxygen atoms. The distinction of macroscopic $I-V$ measurements from the STS measurements in this paper is important to recall while interpreting the switching results obtained here by STS both for TaO_x and for $SrRuO_3$ films.

To understand the switching mechanism in more detail we have switched a larger area on the samples to ON and back to OFF states and examined the electronic structure of the surface in both LRS and HRS. The two states can be spatially distinguished in the STM image and STS data ($I-V$ curves) due to variation in local electronic states. Figure 1a shows the $I-V$ curves taken on HRS (OFF state) and LRS (ON state), which exhibit clear distinctions. $I-V$ curves on LRS showed a higher tunneling current than HRS. The invariable current as a function of voltage at both polarities is due to the current detection limit of our STS setup at approximately 330 nA. Figure 1b–d shows nonintrusive imaging of the initial surface, LRS, and HRS, respectively. The virgin surface (Figure 1b) was reduced at −5 V cathodic tip bias locally on a 200 × 200 nm^2 area (Figure 1c). The contrast change in the STM image can be directly correlated with the resistance change observed in the $I-V$ curve taken on a virgin surface area at voltages beyond −4 V (see Figure S1c). Similarly, application of an anodic polarity (+5 V tip bias) changed the LRS (bright contrast region) to the HRS; that is, the conductance of the initial virgin state of the TaO_x surface is restored (Figure 1d). The reversible switching of the surfaces between LRS and HRS exhibits the desired characteristics of endurance and retention within the experiment time frame. Applying directly an anodic voltage (+5 V tip bias) onto the virgin state never leads to a switching (change of image contrast).

Interestingly, we found a complete reversal of the switching behavior when the TaO_x films were exposed to the atmosphere following the annealing in UHV. In that case, scanning with the same cathodic tip potentials as on the UHV-annealed samples (*i.e.*, −5 V tip bias) did not switch the sample to LRS. Instead, LRS was achieved under +5 V anodic tip potential. As seen from the $I-V$ sweep in Figure 2a, the LRS and HRS states have different band gaps (smaller for LRS) and tunneling currents (larger for LRS). Now the sample can be switched back to HRS under the −5 V cathodic tip potential. The areawise switching on this TaO_x film surface is shown in Figure 2b–d. The switching behavior was repeatable and consistently observed by STM on all samples exposed to the atmosphere after annealing in UHV.

We have performed X-ray photoelectron spectroscopy (XPS) to understand the possible chemical changes leading to such distinctly different switching mechanisms between the two samples: one sample set that was annealed in UHV *versus* the one exposed to the ambient atmosphere after annealing in UHV. Figure 3 shows the changes in Ta 4f photoelectron spectra under different UHV annealing conditions or with aging history. Annealing under UHV conditions reduced the Ta oxidation state, and this effect is more pronounced at higher

DOI: 10.1021/acsnano.5b07020
ACS Nano 2016, 10, 1481–1492

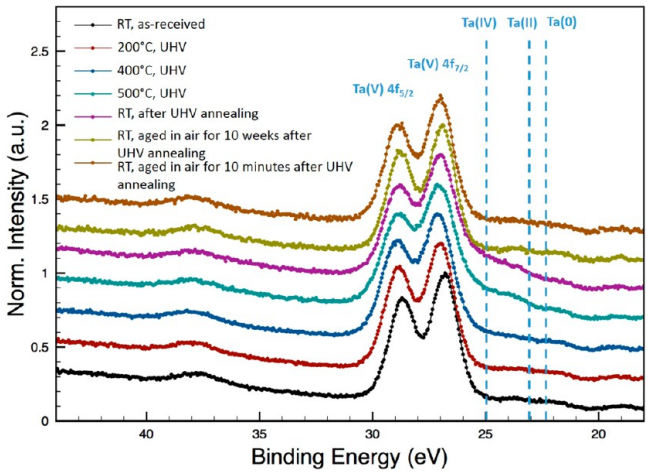

Figure 3. Ta 4f photoelectron spectra at different temperatures in UHV and after exposure to ambient air for different times. Binding energy positions that correspond to Ta^{5+}, Ta^{4+}, Ta^{2+}, and Ta^{0} are marked.

temperatures as expected. The reduced Ta valence states remained after cooling the sample from 500 °C to room temperature (RT) in UHV. However, these states essentially recovered to the as-received more oxidized state upon exposure to ambient air, both after long-term aging (~weeks) as well as after only ~10 min of exposure. A more detailed peak-fitting analysis of the Ta 4f spectra is summarized in Figure S2 in the supplementary data. We found that the Ta in the TaO_x thin film had mixed valence states of Ta^{5+}, Ta^{4+}, Ta^{2+}, and Ta^{0}. Therefore, four sets of Ta 4f doublets were necessary to obtain satisfactory fitting results for the Ta 4f spectrum envelope.[24,25] From the fitting results we conclude that the proportions of reduced Ta^{4+} and Ta^{2+} increased after UHV annealing, indicating an oxygen deficiency introduced in the TaO_x thin film (Figure S3). After exposure to air, the proportions of the reduced Ta valence states changed back roughly to the initial concentrations, within the detection limits of this technique. There are changes in the O 1s peak as well during UHV annealing and after atmosphere exposure (Figure S4). The samples exposed to the atmosphere do not need another UHV annealing step for enabling STM measurements in spite of having a higher proportion of oxidized Ta. Approximately 63% of the collected electrons come from the top 1 nm of the ~2.5 nm thick TaO_x films in this experimental configuration. This indicates that the films reoxidized near the surface while remaining reduced within the bulk of the film, thereby maintaining sufficiently high electronic conductivity for STM after re-exposure to the atmosphere.

The drastic changes in the switching behavior of TaO_x, induced by changes in the sample preparation conditions, indicate a rather complex resistive switching mechanism, with more than one defect species participating in the resistive switching process. Different processes related to oxygen ion/vacancy movement and/or reactions influencing the cell behavior were reported for binary oxides.[26] In our experiments, on the basis of the tip polarity and the corresponding influence on charged defects, the switching behavior of TaO_x films can be described by the following half-cell reactions.

Under cathodic tip potentials (Figure 4a), two reduction reactions can theoretically take place at the TaO_x surface:

$$Ta^{x+} + xe^- \rightarrow Ta \quad (a)$$

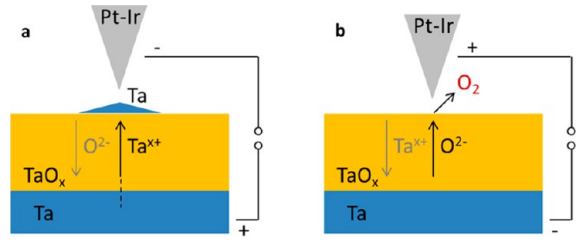

Figure 4. Schematic model of the proposed resistive switching (SET) mechanism of TaO_x thin films under (a) cathodic (reduced samples) and (b) anodic tip potential (air-exposed samples).

$$\frac{1}{2}O_2 + 2e^- \rightarrow O^{2-} \quad (b)$$

Reaction a shows the possibility of the low-resistance state by the reduction of Ta^{x+} ions at the surface. On the other hand, reaction b depends on the oxygen vacancy availability (site balance) to incorporate oxygen ions into the lattice. It is clear that reaction b increases the resistance of the surface by consuming oxygen vacancies.

Similarly, at the bottom electrode (at the interface between TaO_x and Ta metal) the above-mentioned reactions take place in the opposite direction:

$$Ta - xe^- \rightarrow Ta^{x+} \quad (c)$$

$$O^{2-} - 2e^- \rightarrow \frac{1}{2}O_2 \quad (d)$$

Oxidation of Ta metal at the interface (or oxidizing the lattice Ta to higher oxidation states) is possible *via* reaction c. This reaction would increase the resistance of the oxide near the interface. Reaction d creates oxygen vacancies starting at the metal−oxide interface and could lead to lowered resistance of the oxide film if vacancies percolate through the film. However, this reaction would be expected to be hindered given the good contact/adhesion between the Ta bottom electrode and the TaO_x film, limiting the ability of oxygen gas to evolve and lead the solid phase into the gas phase. Such an evolution would be expected to result in gas bubble formation, which was not observed in our experiments.

Under anodic tip potentials (Figure 4b), reactions c and d are theoretically possible at the surface, and reactions a and b at the TaO_x/Ta metal interface. The switching mechanism of this binary oxide is mainly determined by the dominant defect that is contributing for the HRS and the LRS. Next, we reason and explain the switching mechanisms based on thermodynamic arguments, as well as evidence from STM/S for both of the samples that we examined above: the UHV-annealed state and following exposure to the ambient atmosphere.

Switching Mechanism on TaO_x after Annealing in UHV. On the UHV-annealed TaO_x films, when measured in UHV, the switching to LRS (SET) is observed by applying a large cathodic tip potential ($V_{Tip} < -4$ V) with reversal to HRS (RESET) taking place upon application of a large anodic tip potential ($V_{Tip} > 4$ V) (see Figure S1c). As described above, under a cathodic tip potential, Ta^{x+} reduction at the surface (reaction a) and oxygen vacancy creation at the interface (reaction d) are most likely reactions for creating an LRS. The dominant switching mechanism should therefore be defined by the dominant and/or the fast diffusing defect species, *i.e.*, Ta ions or oxygen vacancies. Reactions b and c rather increase the

DOI: 10.1021/acsnano.5b07020
ACS Nano 2016, 10, 1481−1492

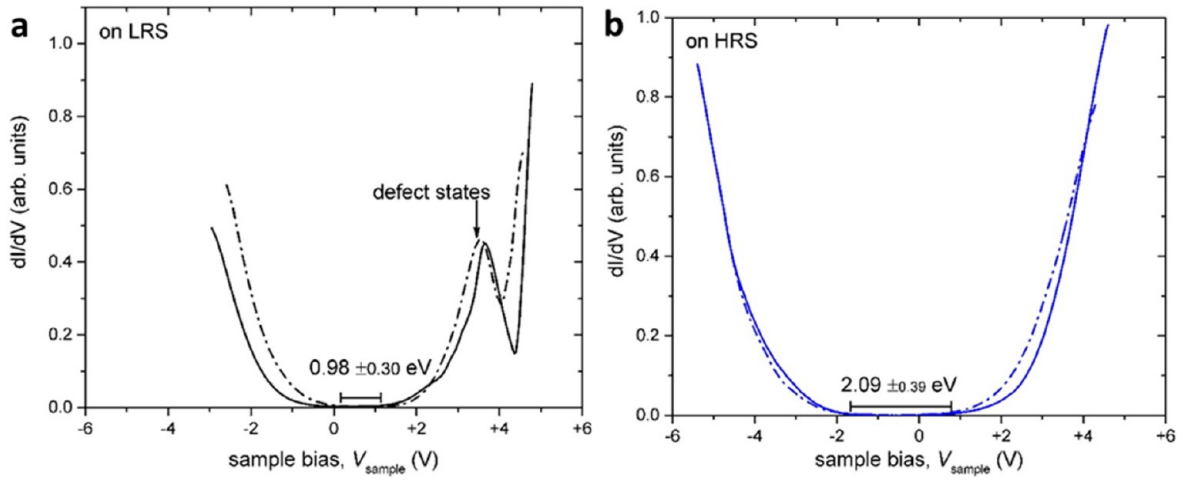

Figure 5. Normalized differential conductivity (dI/dV) spectra measured on TaO_x thin films after exposure to the atmosphere on (a) LRS and (b) HRS. The dashed line represents the average over 10 individual spectra collected at different locations, and the solid line corresponds to a representative dI/dV data set at a single point. The marked band gap values are an approximate measure from the as-collected spectra with $dI/dV \leq 0.02$.

resistance of an n-type nonstoichiometric oxide[27] and mainly contribute to HRS under an anodic tip potential.

Here, for reaction c the standard equilibrium potential of the Ta^{x+}/Ta half-cell reaction is much more negative than that of the oxygen redox reaction d.[28] This means that the oxidation of Ta is thermodynamically more favorable and will proceed first. The Ta^{x+} ions can then enter the TaO_x lattice as interstitials. Alternatively, they can be incorporated into vacant Ta lattice sites or chemically react with oxygen ions from TaO_x, expanding the oxide.

Thus, at both the surface and the buried interface of the TaO_x film, the tantalum cations dominate the redox reactions, but in opposite directions (reduction at the surface and oxidation at the bottom interface). As a consequence, enrichment of metallic tantalum at the surface region leads to higher conductivity (LRS). In support of this explanation, we have observed an ohmic $I-V$ response in our STS experiments (see Figure 1a) indicating no band gap for electron tunneling. This is consistent with Wedig *et al.*'s recent STM study on TaO_x, showing tantalum metal enrichment at the surface under static tip conditions, resulting in a metallic contact to the STM tip with quantum conductance.[23]

Under anodic tip potential (HRS), due to the high oxygen affinity (equilibrium oxygen activity of 10^{-133})[28] of metallic Ta, it can easily oxidize and the HRS can be readily established according to reaction c at the surface. At the interface between TaO_x and the Ta bottom electrode, reactions a and b are both possible, but due to the low oxygen activity at the Ta/TaO_x interface, the reduction of Ta^{x+} to Ta is much more probable. However, in this case the number of Ta ions that can undergo reduction is limited as determined by the excess cations in the TaO_x. Although additional Ta formation by TaO_x decomposition at the surface in principle would be possible, that would lead to destruction of the surface (topography changes due to Ta metal), which has not been observed. Furthermore, the field strength will be lower at the interface in comparison to the surface leading to a lower driving force for reactions a and b to take place.

Therefore, on the basis of phenomenological and experimental evidence, we conclude that the STM-induced ON and OFF states in the UHV-annealed TaO_x films are due to a process of formation/dissolution of metallic Ta, mediated by Ta ions. This process is naturally supported by the oxygen vacancy shift, having the same direction of movement. Thus, we confirm our recent observations, showing a typical ECM type of switching in TaO_x-based devices, explained by Ta ion motion and redox reaction.[23,29] Moreover, formation of Ta filaments,[30] precipitation of Ta metal within TaO_x upon cycling,[31,32] and first-principles calculations confirm metallic Ta is formed and is stable within the TaO_x matrix, leading to metallic conducting filaments.[33]

Switching Mechanism on TaO_x after Exposure to Ambient Atmosphere. Exposing the UHV-annealed TaO_x film to the atmosphere leads to instant oxidation of the TaO_x surface (Figure S3) and also absorption of moisture,[29] and this, we believe, is the main reason for the change of the switching mechanism. The samples exposed to the atmosphere showed LRS after SET with anodic tip potential, *i.e.*, reactions c and d at the surface and reactions a and b at the interface. However, the LRS can be achieved either by reducing Ta^{x+} at the interface (according to reaction a) or creating oxygen vacancies at the surface (according to reaction d). In order to know the fastest diffusing species, tracer diffusion data are needed as a function of stoichiometry. Another important factor is the effect of electric field on defect mobility. However, we have addressed this issue by using STS in differential conductivity mode (dI/dV) *via* a lock-in preamplifier. The dI/dV curves provide information on the local density of states (LDOS). The signature of Ta metal atoms or atom clusters is different from that of oxygen vacancies in the LDOS. In the latter, additional defect states are expected in the band gap, while the former will not have any band gap but exhibit an ohmic $I-V$ shape (as shown in Figure 1a). Figure 5 shows the dI/dV curves measured before and after switching on an atmosphere-exposed (previously UHV-annealed) TaO_x film. It is clear that the band gap decreased significantly in the dI/dV curves of the LRS area (see Figure 5a) in comparison to the HRS area (see Figure 5b). Despite a large error range in the measured band gap values (±0.3 eV), we consistently found a lower band gap on LRS compared to HRS. Further, an additional peak was observed close to the unoccupied states (under positive bias on the sample), indicating defect states in the band gap. Theoretical

DOI: 10.1021/acsnano.5b07020
ACS Nano 2016, 10, 1481−1492

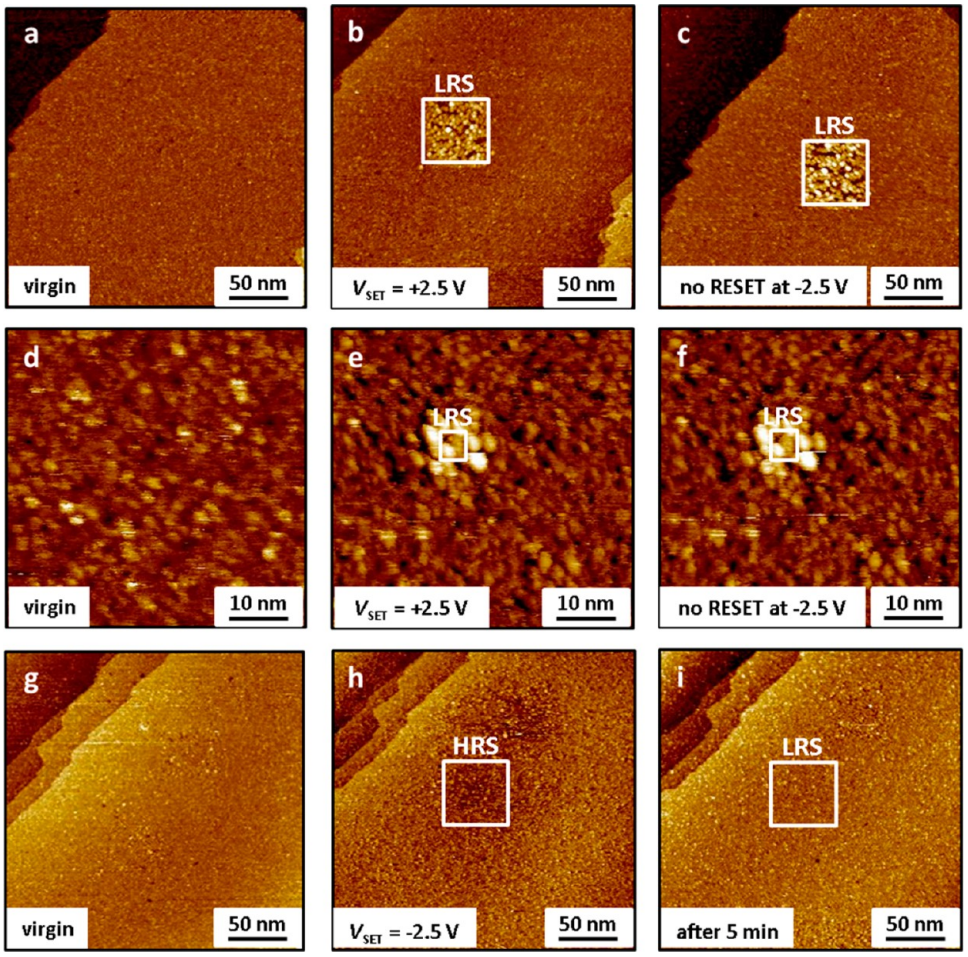

Figure 6. STM images (250 × 250 nm^2, taken with V_{Tip} = −0.5 V, I_T = 1.0 nA) of $SrRuO_3$ film measured (a, d) before and (b, e) after scanning the marked area with V_{Tip} = +2.5 V and I_T = 1.0 nA. (c, f) STM images taken after additionally scanning the marked area with V_{Tip} = −2.5 V and I_T = 1.0 nA following the images shown in (b) and (e). STM images taken (g) before and (h, i) after scanning the marked area with V_{Tip} = −2.5 V and I_T = 1.0 nA. (h) Images taken immediately after and (i) taken 5 min after the attempted switching with V_{Tip} = −2.5 V.

calculations on the hexagonal Ta_2O_5 structure revealed that occupied states mainly correspond to O 2p levels and unoccupied states to Ta 5d and 6s levels.[34,35] Creating oxygen vacancies in the structure leads to an extra peak in LDOS close to the unoccupied states due to electron localization on Ta 5d and 6s states.[34,35] The extra peak found in our experimental dI/dV data is consistent with this computational LDOS analysis on Ta_2O_5. The characteristic peak close to the unoccupied states and smaller band gap on LRS confirm resistive switching by an oxygen vacancy mechanism in these samples different from the UHV-annealed ones, which showed a clear metallic behavior (Figure 1a).[23] Similar to our results here, theoretical work on Ta_2O_5 resistive switching as a function of oxygen non-stoichiometry revealed also distinct mechanisms, *i.e.*, by Ta metal filaments in highly reduced TaO_x and by electron hopping on Ta-rich islands in slightly reduced TaO_x.[32] Similar observations were reported in other oxides,[36−38] where perovskite oxide films always formed defect states below the unoccupied states upon slight reduction, similar to that found in our work.

Resistive Switching on $SrRuO_3$ Induced by the STM Tip. Resistive switching induced by the STM tip bias in a noncontact mode on $SrRuO_3$ was investigated by imaging and I−V measurements, in a similar manner to that described above for the TaO_x films. Figure 6 shows the STM images collected at a tunneling set point of 1 nA and −0.5 V tip bias, without modifying the initial resistance state of the sample. The set parameters are chosen based on the I−V curves over the −3 V to +3 V range, which helped us to define the SET parameters for LRS switching with STM (Figure S7). Figure 6a,b shows the STM image before and after scanning (switching) the marked 50 × 50 nm^2 area with an anodic tip voltage of +2.5 V. After scanning the virgin surface (a) under increased anodic tip potential, the inner area became significantly brighter (in (b)), corresponding to the surface switched to LRS. Unlike the TaO_x films, the brightening effect (LRS) on $SrRuO_3$ is irreversible under UHV conditions; that is, even scanning with a highly negative tip voltage did not recover the virgin image (HRS) (Figure 6c).

An advantage of STM compared to most other scanning probe microscopy methods in inducing electrical switching is its higher spatial resolution capability. This allows one to study switching processes that are usually confined to nanoscale dimensions on the surface of high-quality films. Figure 6d−f shows scanning of a 5 × 5 nm^2 area under anodic tip potential. The LRS (bright) area is around 10 × 10 nm^2 in size (including the granular features), larger than the scanned 5 × 5 nm^2 area. An interesting feature of this area is the uniform brightening of granular features in Figure 6e and f. It is possible to further reduce the scan size under very good imaging conditions, *i.e.*,

DOI: 10.1021/acsnano.5b07020
ACS Nano 2016, 10, 1481−1492

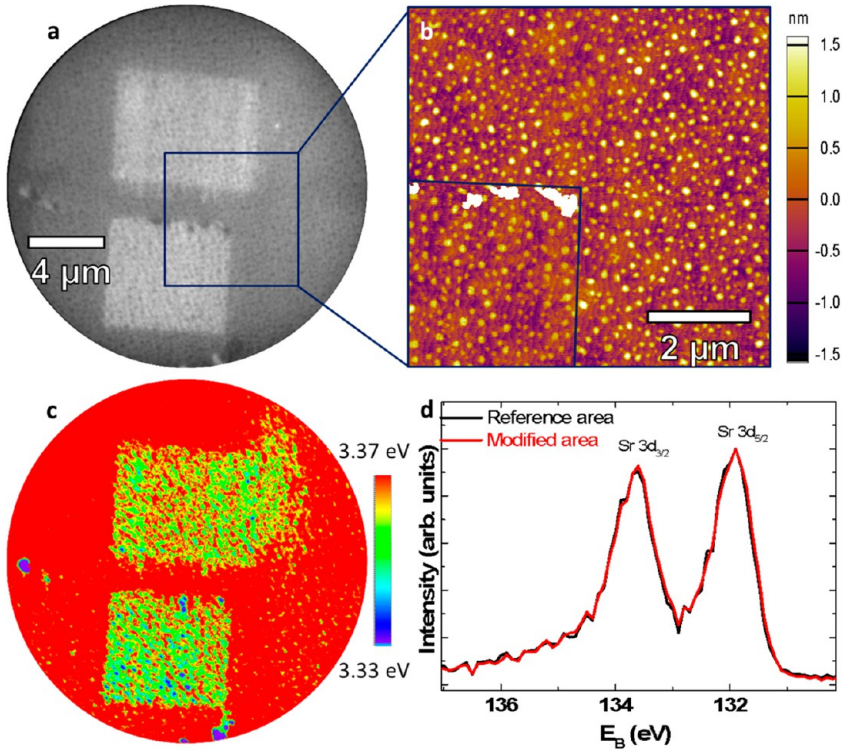

Figure 7. PEEM and AFM data on the two STM-switched areas at the surface of the $SrRuO_3$ film (6.0 × 6.0 μm^2 and 7.0 × 6.0 μm^2, V_{Tip} = +4.0 V; I_T = 1.0 nA): (a) secondary electron contrast map; (b) tapping-mode AFM image (7.0 × 7.0 μm^2) of the area marked in (a); (c) work function contrast map of the area shown in (a); (d) strontium 3d signal intensity inside and outside the switched regions.

clean surface areas with very low roughness and high tip quality. An approximately 2 × 2 nm^2 size of switched area (Figure S8) could be achieved, demonstrating the lower current limit of lateral switching on our samples.

A qualitatively different behavior is observed upon applying a negative tip voltage of −2.5 V to the virgin sample. As shown in Figure 6h, scanning with −2.5 V resulted in the formation of dark regions, inside and around the scanned/marked area that were formerly unmarked (Figure 6g). However, unlike the above case dealing with positive tip voltages, the surface modification (dark area) is not stable and the virgin state is recovered at the zero bias condition within approximately 5 min (Figure 6i).

It can be speculated that the irreversible switching under anodic tip potential may be the consequence of decomposition of the $SrRuO_3$ film caused by the strong electric field of the STM tip (although, below, we will show that a phase decomposition is not taking place here). The decomposition and thermal stability of the $SrRuO_3$ film surface and bulk were thoroughly investigated in the past.[39−44] These references revealed that SrO formation at the surface is inevitable under either reducing or oxidizing atmospheres. Under highly oxidizing conditions, volatile Ru oxides (RuO_4) leave the surface SrO-rich (reaction e), and in extremely reducing atmospheres, metallic Ru and SrO are formed on the surface (reaction f). Under weakly reducing conditions, partial reduction of $SrRuO_3$ into oxygen-deficient $SrRuO_{3-\delta}$ is also possible according to reaction g. These reactions can be represented as follows:

$$SrRuO_3 + O_2 \rightarrow SrO + RuO_4(g) \quad (e)$$

$$SrRuO_3 \rightarrow SrO + Ru + O_2(g) \quad (f)$$

$$SrRuO_3 \rightarrow SrRuO_{3-\delta} + \delta/2O_2(g) \quad (g)$$

Among the three reactions, a change in nonstoichiometry (reaction g) is reversible in the presence of oxygen gas (and irreversible in UHV), and the surface can be recovered upon oxidation treatment without impacting the surface morphology.[39] Ru metal or RuO_4 formation (reactions e and f) is reversible as well in oxygen gas; however these processes can change the surface morphology because of a phase separation of metal or metal-oxide clusters.[39,41] In STM, it would be difficult to resolve the effect of morphology change from the effect of nonstoichiometry and electronic structure. To confirm whether we induced SrO and Ru/RuO_4 phase separation (reactions e and f) or an oxygen-deficient $SrRuO_{3-\delta}$ (reaction g) under anodic tip potential, we analyzed the surface cation chemistry. To deduce the cation composition at the surface, we characterized the STM tip-modified sample surface (bright region) by energy-filtered photoelectron emission microscopy (PEEM) concurrent with AFM measurements. PEEM image stacks of the before STM scanned areas were obtained *in situ* near the photoemission threshold and at the O 1s, Ru 2p, and Sr 3d core levels. Figure 7a shows the secondary electron contrast of these two areas as bright regions (in grayscale), which can be interpreted as a change in the electronic charge density. The slightly lower contrast regions (medium bright in grayscale) around the +4.0 V scans represent the previous readout zones, *i.e.*, areas scanned at a lower tip voltage of −0.5 V. No contrast change was observed on the untreated virgin areas that were not exposed to the STM tip electric field (see Figure 7a, dark region in grayscale). A work function map obtained by fitting the photoemission threshold using an error function[45] is shown in Figure 7c. The two preswitched areas show slightly decreased work functions in comparison to the

DOI: 10.1021/acsnano.5b07020
ACS Nano 2016, 10, 1481−1492

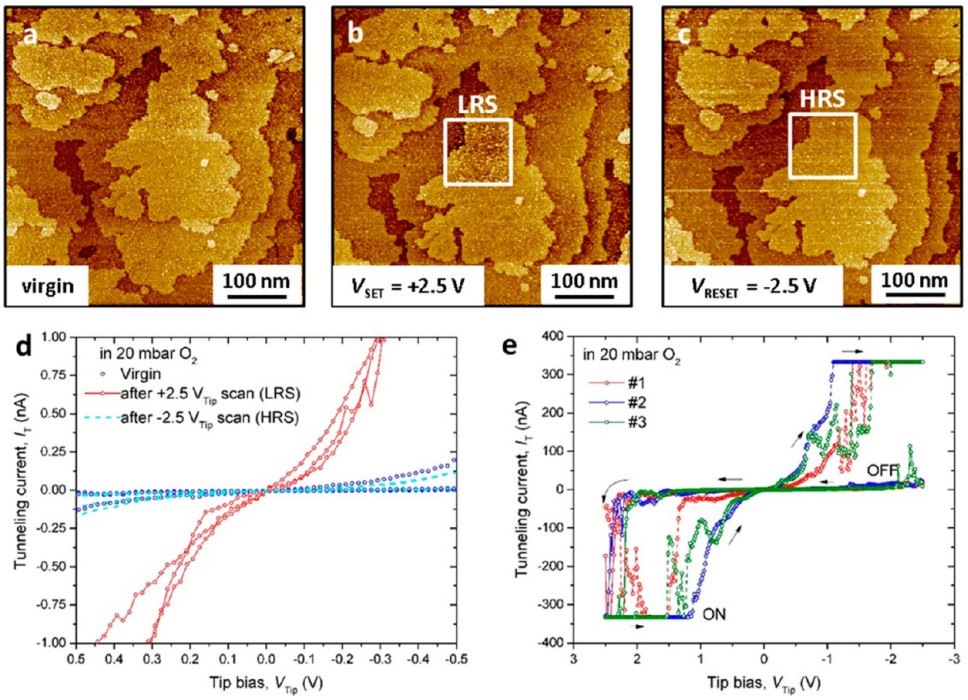

Figure 8. STM images (500 × 500 nm^2, taken at V_{Tip} = −0.3 V, I_T = 0.1 nA) on the $SrRuO_3$ film in an oxygen atmosphere of $p(O_2)$ = 20 mbar, (a) before and (b) after scanning the marked area with V_{Tip} = +2.5 V and I_T = 1.0 nA; (c) after additionally scanning the marked area with V_{Tip} = −2.5 V and I_T = 1.0 nA following the images shown in (b); (d) *I*−*V* data measured at two locations each for the virgin, LRS, and HRS areas on (a), (b), and (c); (e) *I*−*V* sweeps taken on several positions (#1, #2, #3) at the virgin surface.

not switched areas. Comparing the Sr 3d core level peaks in Figure 7d taken inside and outside the switched areas, no significant differences in peak position or shape are exhibited, excluding the possibility of $SrRuO_3$ film decomposition during switching under anodic tip voltages. Both O 1s and Ru 2p X-ray photoelectron spectra for the same regions also do not indicate decomposition (Figure S9). From these data, Ru/Sr ratios of 0.171 and 0.176 were calculated for inside and outside the switched regions, respectively, essentially providing no indication of phase separation. The Me/O ratios of 0.26 inside and 0.34 outside the switched areas, respectively, can be interpreted by either reaction f or g. However, the intensity distribution of the O 1s peaks also indicates a cleaning effect of the STM tip. Thus, the slight difference in work function energies should be due to a change of the electronic properties (correlated either to different adsorbate coverages or, more likely, to the oxygen nonstoichiometry) caused by the STM tip induced field. Apart from some bigger particles near the outer borders of one of the switched zones in the AFM scans (Figure 7b), the surface morphology appears to be identical inside and outside the switched areas. Therefore, the changes in work function cannot be caused by a different morphology of the anodic switched surface areas, which eliminates reaction f.

The STM and AFM images of the surface of $SrRuO_3$ films look sharp both before and after the tip-induced switching (see Figures 6 and 7) and are overall consistent with each other. The AFM images on the STM-switched area revealed no topography/depth changes due to the applied electric field at +4 V tip potential. On the basis of the PEEM and AFM results, we conclude that the contrast change found in STM (Figure 6) after scanning with a high anodic tip potential is not due to phase decomposition at the surface. It appears that a nonstoichiometry change within $SrRuO_{3-\delta}$ is more likely, *i.e.*, loss of lattice oxygen from $SrRuO_3$ under anodic tip potential (reaction g) in UHV. The observed effect is then irreversible under cathodic tip potential due to the unavailability of oxygen molecules (Figure 6c) to be reincorporated into the $SrRuO_{3-\delta}$ film under UHV conditions. In order to verify this mechanism, we have performed STM/S to investigate the switching mechanism of $SrRuO_3$ under increased oxygen partial pressures, pO_2, within the reach of our instrument operating conditions.

Resistive Switching on $SrRuO_3$ Induced by the STM Tip under High-$p(O_2)$ Conditions. To investigate the possibility of reversibly switching the $SrRuO_3$ films, measurements were instead repeated under 20 mbar $p(O_2)$ in the STM chamber. Figure 8a shows the STM image of the virgin surface at a tunneling set point of −0.3 V tip bias and 0.1 nA. It is possible to resolve the atomic terraces in these films even under such high-$p(O_2)$ conditions. Figure 8b shows the effect of +2.5 V anodic tip potential on the virgin surface, forming a bright contrast (LRS) in the STM image. Figure 8a,b images are comparable to the effects noticed under UHV conditions described in Figure 6. However, in contrast to the results obtained under UHV conditions, scanning the LRS area with a cathodic tip potential of −2.5 V recovered the surface to its virgin (HRS) state (Figure 8c). This shows that the availability of oxygen at the surface is necessary to return the resistance state from LRS back to HRS. The reversible switching phenomena under these conditions are highly repeatable. To explain our results more quantitatively, STS was performed on the virgin state, after scanning with a high anodic and after scanning with a high cathodic tip bias. Figure 8d shows the initial low tunneling current (HRS) in the *I*−*V* data of the virgin state, the increase in tunneling current (LRS) on the regions SET with an anodic tip bias (+2.5 V), and the decrease in tunneling current (HRS) after RESET with a cathodic tip bias (−2.5 V). *I*−*V* sweeps collected at various positions by

DOI: 10.1021/acsnano.5b07020
ACS Nano 2016, 10, 1481−1492

turning off the feedback loop showed a typical memristive hysteresis (see Figure 8e).

Switching Mechanism on $SrRuO_3$. Based on the STM studies performed both in UHV and at high oxygen partial pressure, it is evident that oxygen vacancies play a vital role in the electrical switching of $SrRuO_3$ thin films. The resistive switching mechanism can be described as follows:

(1) In case of an anodic tip potential (Figure 9a) and UHV conditions, oxygen ions are oxidized at the surface, forming molecular oxygen (reaction d), which then desorbs into the vacuum and is irreversibly lost. The electrical and structural properties of $SrRuO_3$ are very sensitive to the oxygen nonstoichiometry in the material.[46−48] However, the point defect chemistry of $SrRuO_3$ has not been thoroughly studied to date based on an examination of the available literature. Comparing $SrRuO_3$ with other perovskite materials, we can expect that oxygen-rich $SrRuO_3$, like in the case of our virgin films, behaves as p-type conducting, showing an electrical conductivity increase due to the generation of electron holes associated with oxygen vacancy annihilation, whereas oxygen-deficient $SrRuO_{3-\delta}$ films formed under highly reducing conditions are dominated by n-type conduction, increasing their electrical conductivity by the generation of additional oxygen vacancies and electrons. At intermediate oxygen partial pressure, the conductivity should go through a minimum for conditions at which n ≈ p. Alternatively, the transition from p- to n-type conductivity can occur abruptly driven by structural lattice distortion (again driven by loss of oxygen). For example, Lu *et al.*[48] explained the conductivity increase in oxygen-deficient thin films (with the oxygen vacancy concentration) based on the increase of orbital overlap of Ru 4d and O 2p states, as found by density functional theory calculations.

Thus, at anodic tip potentials, which evolve oxygen from the $SrRuO_3$ lattice and increase the oxygen vacancy concentration, we can expect the domination of n-type conduction and observe an electronic conductivity increase of our films (Figure 9a).

(2) Under cathodic tip potential, oxygen reduction reaction (reaction b) or Ru reduction is possible at the $SrRuO_3$ surface (Figure 9b). On the basis of our high-$p(O_2)$ STM measurements and STS data (Figure 8), it is evident that a RESET to HRS and, thus, reversible switching are achieved only when there are oxygen molecules available in the chamber, overruling the formation of Ru metal. In the case of measurements under UHV, the unavailability of oxygen in the chamber limited this reaction.

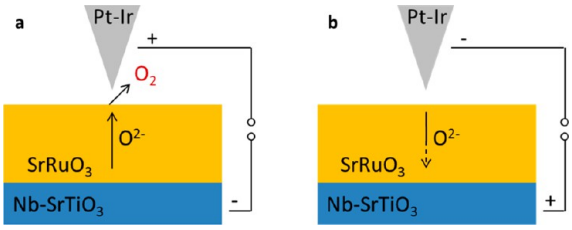

Figure 9. Schematic model of the proposed resistive switching mechanism on $SrRuO_3$ thin films under (a) anodic and (b) cathodic tip potentials.

Exposing the more oxygen-rich and, thus, p-conducting virgin film surface to cathodic tip potential in UHV showed a time-dependent disappearance of the dark areas (Figure 6h,i). This is likely due to a redistribution of the oxygen vacancies toward the surface under the applied electric field (however, a charge-trapping effect cannot be unequivocally ruled out). As soon as the applied field is turned off, the vacancy concentration redistributes to equilibrate across the film, recovering the conductance of the virgin surface. A similar effect has been reported for $SrTiO_3$.[49] Such a behavior is also in accordance with a recent work of Setvin *et al.*, who observed an enrichment of oxygen vacancies on the TiO_2 anatase (101) surface under high cathodic STM tip potentials.[50] At temperatures above 200 K, the vacancies redistributed very soon after the applied electric field was turned off. Their explanation of "hot electron injection" as a driving force for the vacancy movement may also be valid for the virgin $SrRuO_3$ surface. However, the dependence of the switching process on the oxygen partial pressure supports more an explanation involving the increase of the oxygen vacancy mobility caused by enhanced oxygen depletion in the $SrRuO_3$.[51]

Lastly we note that it is of fundamental interest for the community that a material like $SrRuO_3$, which is expected to act as a purely electronic conductor in ReRAM electrodes, shows resistive switching behavior based on anion motion. This may have a significant influence on the device switching properties impacted by the electrolyte−electrode interfaces.

CONCLUSIONS

We have used STM and STS to reveal the resistive switching mechanisms in electronically distinct oxide systems. We demonstrated local resistive switching of TaO_x and $SrRuO_3$ thin films with an STM tip, without necessitating a top electrode in physical contact with the surface. STM and STS together helped us to probe the bare surface and investigate the mechanisms underlying the electronic switching in these materials. Resistive switching in TaO_x thin films strongly depends on the nonstoichiometry that is affected by the sample history. In the case of highly reduced TaO_x films, the low-resistance state is achieved under cathodic tip potential by reducing TaO_x locally to Ta metal. In contrast, reoxidized films exposed to the atmosphere showed a low-resistance state under anodic tip potential by creating oxygen vacancies. We could correlate the electronic state in the LRS condition to the presence of Ta metal or of oxygen vacancy defect states in the density of states measured by STS. $SrRuO_3$ thin films showed resistive switching *via* oxidation/reduction and migration of oxygen ions, and the reversibility of switching was achieved only under high oxygen pressure. The irreversible switching of $SrRuO_3$ under anodic tip potential in UHV conditions further supports the role of oxygen vacancies for resistive switching. On the basis of these two systems, we believe the nonstoichiometry of the oxides determines the switching mechanism in valence change memories. Although the investigated systems differ strongly in their electronic and structural properties, the combination of STM and STS measurements with other surface science techniques allowed us to determine the governing mechanisms behind the electronic switching in these materials. This demonstrates the power of STM for

DOI: 10.1021/acsnano.5b07020
ACS Nano 2016, 10, 1481−1492

elucidating resistive switching phenomena across a wide spectrum of transition metal oxides.

METHODS

Sample Preparation. TaO_x thin films of approximately 2.5 nm thickness were deposited at room temperature on Ta (50 nm)/SiO_2/Si substrates *via* reactive sputtering. In the initial step, a 50 nm thick tantalum film was sputter-deposited on a SiO_2/Si wafer from a metallic target with 30 W power in a pure argon atmosphere at a partial pressure of 7×10^{-3} mbar. To achieve thin Ta_2O_{5-x} films on an existing Ta film, the chamber pressure was increased to 3.5×10^{-2} mbar by releasing O_2 (75% Ar and 25% O_2) and lowering the sputtering power to 20 W. A Pt stripe was deposited by a lift-off process on one side of the device contacting the Ta metal to serve as the bottom contact for STM studies (Figure S10). The as-deposited TaO_x samples were insulating (Figure S1), and the surface conductivity was increased by preannealing under UHV conditions ($\sim 10^{-10}$ mbar) at approximately 500 °C for 2−3 h prior to the STM investigation.

$SrRuO_3$ thin films of 10 nm thickness were grown epitaxially on Nb-doped $SrTiO_3$ substrates by pulsed layer deposition with a laser energy of 0.6 J/cm^2 at a 10 Hz repetition rate. During deposition the substrate was maintained at 650 °C in an oxygen partial pressure of 0.13 mbar. After deposition the sample was slowly cooled to room temperature under a higher oxygen partial pressure of 0.5 mbar. The conductive substrate (Nb-doped $SrTiO_3$) served as the bottom electrode or ground for the STM measurements.

Scanning Tunneling Microscopy. The STM and STS experiments were performed at room temperature in an Omicron VT-SPM system operated at 5×10^{-10} mbar base pressure. For high oxygen partial pressure (~20 mbar) studies, the chamber was isolated from the vacuum system and O_2 was released into the chamber. For imaging and current−voltage spectroscopy mechanically cut or electrochemically etched Pt−Ir tips were used. For differential conductivity (dI/dV) measurements, a lock-in preamplifier was used to increase the signal-to-noise ratio. The STM data were analyzed with the SPIP program from Image Metrology.

X-ray Photoelectron Spectroscopy. X-ray photoelectron spectroscopy on TaO_x thin films was utilized to determine the Ta valence state at elevated temperatures under UHV conditions and after aging in air. An Omicron EA 125 hemispherical analyzer and an Omicron DAR 400 Mg/Al dual anode X-ray source were used to perform XPS measurements (Al anode used in this work). CasaXPS software was used for peak fitting and quantification. The as-received films had been originally annealed under vacuum conditions and were then stored for several weeks in air before usage. Ta 4f and O 1s spectra were acquired at room temperature and then at elevated temperatures (200, 400, and 500 °C) *in situ* in UHV (base pressure $\approx 6 \times 10^{-9}$ mbar), with an emission angle of 60°. The inelastic mean free path of the Ta 4f photoelectrons is ~2.2 nm, and approximately 63% of the collected electrons come from the top 1 nm. After vacuum annealing at 500 °C the sample was cooled to RT in UHV and another spectrum was acquired to understand the effect of UHV annealing on the Ta oxidation state. In order to understand the effect of aging in an air atmosphere, extra XPS measurements were performed on another two samples. The first sample was aged in an air atmosphere for about 2 weeks and then transferred into the UHV chamber for XPS measurements at RT. The second sample was first annealed in the UHV chamber, then exposed to air for a very short period of time (~10 min), and finally transferred back into the UHV chamber for measurements.

X-ray Photoelectron Emission Microscopy. XPEEM was used to examine the chemical composition of the $SrRuO_3$ films. Measurements were performed with a NanoESCA (Omicron Nanotechnology GmbH, Taunusstein, Germany) operated in aberration-corrected energy-filtered imaging ESCA mode with Al K_alpha X-ray illumination. The lateral resolution for core level imaging was estimated to be 0.4 μm. The total energy resolution determined from both the spectrometer broadening (the pass energy 100 eV and the entrance slit 1 mm) and the photon bandwidth was 400 meV for photoemission spectra. A series of images were taken at increasing binding energies of Sr 3d, Ru 3p, and O 1s core level photoelectrons with steps of 0.1 eV. The respective photoemission spectra were extracted from the resulting image stack in different regions of interest. The image stacks were analyzed, and spectra were extracted using the IGOR Pro Software.

Atomic Force Microscopy. The AFM measurements were performed at room temperature and under ambient conditions using the Cypher atomic force microscope from Asylum Research (Santa Barbara, CA, USA) operated in tapping mode. For the measurements silicon cantilevers from Nanoworld (ARROW-NCR-50) with a spring constant of 42 N/m were used.

ASSOCIATED CONTENT

Supporting Information

The Supporting Information is available free of charge on the ACS Publications website at DOI: 10.1021/acsnano.5b07020.

STM measurements on TaOx films; detailed analyses of XPS measurements on TaOx films; STS measurements on $SrRuO_3$ films; STM imaging; PEEM data; schematic structure of the samples used for STM experiments with TaO_x (PDF)

AUTHOR INFORMATION

Corresponding Authors

*E-mail: byildiz@mit.edu.
*E-mail: i.valov@fz-juelich.de.

Author Contributions

⊥M. Moors and K. K. Adepalli contributed equally.

Notes

The authors declare no competing financial interest.

ACKNOWLEDGMENTS

K.K.A., H.T., and B.Y. thank the National Science Foundation for support through the MIT Center of Materials Science and Engineering MRSEC under grant no. DMR-1419807. The work was also financially supported in part by BMBF project no. 03X0140 and DFG priority program SFB 917. K.S. has been supported by the Initiative and Networking Fund of the German Helmholtz Association, Helmholtz Virtual Institute VH-VI-442 MEMRIOX. C.B. and R.D. also acknowledge funding from the W2/W3 program of the Helmholtz Association.

REFERENCES

(1) Waser, R.; Aono, M. Nanoionics-based Resistive Switching Memories. *Nat. Mater.* **2007**, *6*, 833−840.

(2) Yang, J. J.; Strukov, D. B.; Stewart, D. R. Memristive Devices for Computing. *Nat. Nanotechnol.* **2013**, *8*, 13−24.

(3) Waser, R.; Bruchhaus, R.; Menzel, S. *Redox-Based Resistive Switching Memories*; Wiley-VCH, 2012; pp 683−710.

(4) Wei, Z.; Takagi, T.; Kanzawa, Y.; Katoh, Y.; Ninomiya, T.; Kawai, K.; Muraoka, S.; Mitani, S.; Katayama, K.; Fujii, S.; Miyanaga, R.; Kawashima, Y.; Mikawa, T.; Shimakawa, K.; Aono, K. Retention Model for High-Density ReRAM. In *2012 4th IEEE International Memory Workshop, IMW 2012*; 2012 4th IEEE International Memory Workshop, 2012.

(5) Sawa, A. Resistive Switching in Transition Metal Oxides. *Mater. Today* **2008**, *11*, 28−36.

(6) Valov, I. Redox-Based Resistive Switching Memories (ReRAMs): Electrochemical Systems at the Atomic Scale. *ChemElectroChem* **2014**, *1*, 26−36.

DOI: 10.1021/acsnano.5b07020
ACS Nano 2016, 10, 1481−1492

(7) Kwon, D.-H.; Kim, K. M.; Jang, J. H.; Jeon, J. M.; Lee, M. H.; Kim, G. H.; Li, X.-S.; Park, G.-S.; Lee, B.; Han, S.; Kim, M.; Hwang, C. S. Atomic Structure of Conducting Nanofilaments in TiO_2 Resistive Switching Memories. *Nat. Nanotechnol.* **2010**, *5*, 148−153.
(8) Yang, Y.; Gao, P.; Li, L.; Pan, X.; Tappertzhofen, S.; Choi, S.; Waser, R.; Valov, I.; Lu, W. D. Electrochemical Dynamics of Nanoscale Metallic Inclusions in Dielectrics. *Nat. Commun.* **2014**, *5*, 4232.
(9) Celano, U.; Goux, L.; Belmonte, A.; Opsomer, K.; Franquet, A.; Schulze, A.; Detavernier, C.; Richard, O.; Bender, H.; Jurczak, M.; Vandervorst, W. Three-Dimensional Observation of the Conductive Filament in Nanoscaled Resistive Memory Devices. *Nano Lett.* **2014**, *14*, 2401−2406.
(10) Szot, K.; Speier, W.; Bihlmayer, G.; Waser, R. Switching the Electrical Resistance of Individual Dislocations in Single-Crystalline $SrTiO_3$. *Nat. Mater.* **2006**, *5*, 312−320.
(11) Nayak, A.; Wang, Q.; Itoh, Y.; Tsuruoka, T.; Hasegawa, T.; Boodhoo, L.; Mizuta, H.; Aono, M. Position, Detection and Observation of a Conducting Filament Hidden under a Top Electrode in a Ta_2O_5-based Atomic Switch. *Nanotechnology* **2015**, *26*, 145702.
(12) Dittmann, R.; Muenstermann, R.; Krug, I.; Park, D.; Menke, T.; Mayer, J.; Besmehn, A.; Kronast, F.; Schneider, C. M.; Waser, R. Scaling Potential of Local Redox Processes in Memristive $SrTiO_3$ Thin-Film Devices. *Proc. IEEE* **2012**, *100*, 1979−1990.
(13) Choi, B. J.; Jeong, D. S.; Kim, S. K.; Rohde, C.; Choi, S.; Oh, J. H.; Kim, H. J.; Hwang, C. S.; Szot, K.; Waser, R.; Reichenberg, B.; Tiedke, S. Resistive Switching Mechanism of TiO_2 Thin Films Grown by Atomic-Layer Deposition. *J. Appl. Phys.* **2005**, *98*, 33715.
(14) Bersuker, G.; Gilmer, D. C.; Veksler, D.; Kirsch, P.; Vandelli, L.; Padovani, A.; Larcher, L.; McKenna, K.; Shluger, A.; Iglesias, V.; Porti, M.; Nafria, M. Metal Oxide Resistive Memory Switching Mechanism Based on Conductive Filament Properties. *J. Appl. Phys.* **2011**, *110*, 124518.
(15) Lee, M. H.; Hwang, C. S. Resistive Switching Memories: Observations with Scanning Probe Microscopy. *Nanoscale* **2011**, *3*, 490−502.
(16) Nardi, F.; Deleruyelle, D.; Spiga, S.; Muller, C.; Bouteille, B.; Ielmini, D. Switching of Nanosized Filaments in NiO by Conductive Atomic Force Microscopy. *J. Appl. Phys.* **2012**, *112*, 64310.
(17) Terabe, K.; Hasegawa, T.; Nakayama, T.; Aono, M. Quantized Conductance Atomic Switch. *Nature* **2005**, *433*, 47−50.
(18) Nayak, A.; Tamura, T.; Tsuruoka, T.; Terabe, K.; Hosaka, S.; Hasegawa, T.; Aono, M. Rate-Limiting Processes Determining the Switching Time in a Ag_2S Atomic Switch. *J. Phys. Chem. Lett.* **2010**, *1*, 604−608.
(19) Valov, I.; Sapezanskaia, I.; Nayak, A.; Tsuruoka, T.; Bredow, T.; Hasegawa, T.; Staikov, G.; Aono, M.; Waser, R. Atomically Controlled Electrochemical Nucleation at Superionic Solid Electrolyte Surfaces. *Nat. Mater.* **2012**, *11*, 530−535.
(20) Nayak, A.; Tsuruoka, T.; Terabe, K.; Hasegawa, T.; Aono, M. Switching Kinetics of a Cu_2S-based Gap-type Atomic Switch. *Nanotechnology* **2011**, *22*, 235201.
(21) Chen, Y. L.; Wang, J.; Xiong, C. M.; Dou, R. F.; Yang, J. Y.; Nie, J. C. Scanning Tunneling Microscopy/Spectroscopy Studies of Resistive Switching in Nb-doped $SrTiO_3$. *J. Appl. Phys.* **2012**, *112*, 023703.
(22) Mehonic, A.; Cueff, S.; Wojdak, M.; Hudziak, S.; Labbé, C.; Rizk, R.; Kenyon, A. J. Electrically Tailored Resistance Switching in Silicon Oxide. *Nanotechnology* **2012**, *23*, 455201.
(23) Wedig, A.; Luebben, M.; Cho, D.-Y.; Moors, M.; Skaja, K.; Rana, V.; Hasegawa, T.; Adepalli, K.; Yildiz, B.; Waser, R.; Valov, I. Nanoscale Cation Motion in TaO_x, HfO_x and TiO_x Memristive Systems Reveals Fundamentally Different Switching Models. *Nat. Nanotechnol.* **2016**, *11*, 67−74.
(24) Kerrec, O.; Devilliers, D.; Groult, H.; Marcus, P. Study of Dry and Electrogenerated Ta_2O_5 and $Ta/Ta_2O_5/Pt$ structures by XPS. *Mater. Sci. Eng., B* **1998**, *55*, 134−142.
(25) Demiryont, H.; Sites, J. R.; Geib, K. Effects of Oxygen Content on the Optical Properties of Tantalum Oxide Films Deposited by Ion-Beam Sputtering. *Appl. Opt.* **1985**, *24*, 490.
(26) Yang, J. J.; Miao, F.; Pickett, M. D.; Ohlberg, D. A. A.; Stewart, D. R.; Lau, C. N.; Williams, R. S. The mechanism of electroforming of metal oxide memristive switches. *Nanotechnology* **2009**, *20*, 215201.
(27) Kofstad, P. On The Defect Structure of Ta_2O_5. *J. Electrochem. Soc.* **1962**, *109*, 776−781.
(28) Vanysek, P. *Electrochemicals Series*, 88th ed. 2008.
(29) Lübben, M.; Karakolis, P.; Ioannou-Sougleridis, V.; Normand, P.; Dimitrakis, P.; Valov, I. Graphene-Modified Interface Controls Transition from VCM to ECM Switching Modes in Ta/TaO_x Based Memristive Devices. *Adv. Mater.* **2015**, *27*, 6202−6207.
(30) Yang, M.; Ju, H.; Kim, G. H.; Lee, J.; Ryu, H. Direct evidence on Ta-Metal Phases Igniting Resistive Switching in TaO_x Thin Film. *Sci. Rep.* **2015**, *5*, 14053.
(31) Lee, M.-J.; Lee, C. B.; Lee, D.; Lee, S. R.; Chang, M.; Hur, J. H.; Kim, Y.-B.; Kim, C.-J.; Seo, D. H.; Seo, S.; Chung, U.-I.; Yoo, I.-K.; Kim, K. A Fast, High-Endurance and Scalable Non-Volatile Memory Device Made from Asymmetric Ta_2O_{5-x}/TaO_{2-x} Bilayer Structures. *Nat. Mater.* **2011**, *10*, 625−630.
(32) Strachan, J. P.; Medeiros-Ribeiro, G.; Yang, J. J.; Zhang, M.-X.; Miao, F.; Goldfarb, I.; Holt, M.; Rose, V.; Williams, R. S. Spectromicroscopy of Tantalum Oxide Memristors. *Appl. Phys. Lett.* **2011**, *98*, 242114.
(33) Xiao, B.; Watanabe, S. Oxygen Vacancy Effects on an Amorphous TaO_x-based Resistance Switch: A First Principles Study. *Nanoscale* **2014**, *6*, 10169−10178.
(34) Sawada, H.; Kawakami, K. Electronic Structure of Oxygen Vacancies in Ta_2O_5. *J. Appl. Phys.* **1999**, *86*, 956.
(35) Ivanov, M. V.; Perevalov, T. V.; Aliev, V. S.; Gritsenko, V. A.; Kaichev, V. V. Electronic Structure of d-Ta_2O_5 with Oxygen Vacancies: *ab initio* Calculations and Comparison with Experiment. *J. Appl. Phys.* **2011**, *110*, 024115.
(36) Sitaputra, W.; Skowronski, M.; Feenstra, R. M. Topographic and Electronic Structure of Cleaved $SrTiO_3(001)$ Surfaces. *J. Vac. Sci. Technol., A* **2015**, *33*, 031402.
(37) Sitaputra, W.; Sivadas, N.; Skowronski, M.; Xiao, D.; Feenstra, R. M. Oxygen Vacancies on SrO-Terminated $SrTiO_3(001)$ Surfaces Studied by Scanning Tunneling Spectroscopy. *Phys. Rev. B: Condens. Matter Mater. Phys.* **2015**, *91*, 205408.
(38) Bonnell, D. Scanning Tunneling Microscopy and Spectroscopy of Oxide Surfaces. *Prog. Surf. Sci.* **1998**, *57*, 187−252.
(39) Bensch, W.; Schmalle, H. W.; Reller, A. Structure and Thermochemical Reactivity of $CaRuO_3$ and $SrRuO_3$. *Solid State Ionics* **1990**, *43*, 171−177.
(40) Lee, H. N.; Christen, H. M.; Chisholm, M. F.; Rouleau, C. M.; Lowndes, D. H. Thermal Stability of Epitaxial $SrRuO_3$ Films as a Function of Oxygen Pressure. *Appl. Phys. Lett.* **2004**, *84*, 4107−4109.
(41) Shin, J.; Kalinin, S. V.; Lee, H. N.; Christen, H. M.; Moore, R. G.; Plummer, E. W.; Baddorf, A. P. Surface Stability of Epitaxial $SrRuO_3$ Films. *Surf. Sci.* **2005**, *581*, 118−132.
(42) Halley, D.; Rossel, C.; Widmer, D.; Wolf, H.; Gariglio, S. Thermal Stability of $SrRuO_3$ Epitaxial Layers under Forming-Gas Anneal. *Mater. Sci. Eng., B* **2004**, *109*, 113−116.
(43) Shin, J.; Kalinin, S.; Lee, H.; Christen, H.; Moore, R.; Plummer, E.; Baddorf, A. Surface Stability of Epitaxial $SrRuO_3$ Thin Films in Vacuum. *J. Mater. Res.* **2004**, *19*, 3447.
(44) Mlynarczyk, M.; Szot, K.; Petraru, A.; Poppe, U.; Breuer, U.; Waser, R.; Tomala, K. Surface Layer of $SrRuO_3$ Epitaxial Thin Films under Oxidizing and Reducing Conditions. *J. Appl. Phys.* **2007**, *101*, 23701.
(45) Mathieu, C.; Barrett, N.; Rault, J.; Mi, Y. Y.; Zhang, B.; De Heer, W. A.; Berger, C.; Conrad, H. E.; Renault, O. Microscopic Correlation between Chemical and Electronic States in Epitaxial Graphene on SiC(000−1). *Phys. Rev. B: Condens. Matter Mater. Phys.* **2011**, *83*, 235436.
(46) Maria, J.-P.; Trolier-McKinstry, S.; Schlom, D. G.; Hawley, M. E.; Brown, G. W. The Influence of Energetic Bombardment on the Structure and Properties of Epitaxial $SrRuO_3$ Thin Films Grown by Pulsed Laser Deposition. *J. Appl. Phys.* **1998**, *83*, 4373−4379.

DOI: 10.1021/acsnano.5b07020
ACS Nano 2016, 10, 1481−1492

(47) Yoo, Y. Z.; Chmaissem, O.; Kolesnik, S.; Dabrowski, B.; Maxwell, M.; Kimball, C. W.; McAnelly, L.; Haji-Sheikh, M.; Genis, A. P. Contribution of Oxygen Partial Pressures Investigated over a Wide Range to $SrRuO_3$ Thin-Film Properties in Laser Deposition Processing. *J. Appl. Phys.* **2005**, *97*, 103525.
(48) Lu, W.; He, K.; Song, W.; Sun, C. J.; Chow, G. M.; Chen, J. s. Effect of Oxygen Vacancies on the Electronic Structure and Transport Properties of $SrRuO_3$ Thin Films. *J. Appl. Phys.* **2013**, *113*, 17E125.
(49) Andrä, M.; Gunkel, F.; Bäumer, C.; Xu, C.; Dittmann, R.; Waser, R. The Influence of the Local Oxygen Vacancy Concentration on the Piezoresponse of Strontium Titanate Thin Films. *Nanoscale* **2015**, *7*, 14351−14357.
(50) Setvin, M.; Schmid, M.; Diebold, U. Aggregation and Electronically Induced Migration of Oxygen Vacancies in TiO_2 Anatase. *Phys. Rev. B: Condens. Matter Mater. Phys.* **2015**, *91*, 195403.
(51) Schraknepper, H.; Baumer, C.; Dittmann, R.; De Souza, R. A. Complex Behavior of Vacancy Point-Defects in $SrRuO_3$ Thin Films. *Phys. Chem. Chem. Phys.* **2015**, *17*, 1060−1069.

DOI: 10.1021/acsnano.5b07020
ACS Nano 2016, 10, 1481−1492